Proceedings of the 21st ICSMGE, Vienna, Austria, 14 – 19 June 2026. Pistrol, Adam & Schweiger (eds.)
Published by: ÖGG, Austrian Society for Geomechanics, Salzburg, Austria, ISBN 978-3-9503898-4-5
https://doi.org/10.53243/ICSMGE2026-103

Accelerated implicit cyclic loading with an interface implementation

Tomáš Kadlíček, Stanislav Pařez, David Mašín
Faculty of Science, Charles University, Czech Republic, tomas.kadlicek@natur.cuni.cz.

ABSTRACT: Simulation of cyclic loading can be approached with two types of numerical strategies. The first, designated as the implicit cyclic loading, uses a constitutive model to simulate each individual cycle in its full extent. This strategy is significantly computationally demanding even when simulating higher hundreds to lower thousands of cycles. This issue becomes even more pronounced when contemporary advanced constitutive models are used, which have to meet strict time integration constraints. The second, called the explicit cyclic loading, simulates only average values of each cycle, and the constitutive models used are closely related to constitutive models of creep. Although these models show fast calculation speed, their use is limited by the maximum strain amplitude $\Delta\varepsilon < 0.001$, and they do not reliably follow the limiting states. To improve the main drawback of the implicit cyclic loading, i.e., its calculation speed, we pursue a numerical acceleration based on an extrapolation of all state variables and nodal displacements, resulting in instantaneous jumps during the implicit cyclic loading. In this contribution, we show a study of the acceleration on a laterally loaded pile, where the pile is represented by the linear elastic model, soil is represented by the hypoplastic sand model, and the interface is represented by the Mohr-Coulomb model. All three models are thus accelerated simultaneously at times.

KEYWORDS: Implicit, cyclic loading, acceleration, numerical modelling.

1 INTRODUCTION

In the last decade, the investigation into the mechanical cyclic loading of soils has been one of the most critical fields of research in the geotechnology. One of the driving forces in this pursuit is the transformation of the energy sector and growth of energy wind farms. These structures are subjected to a lifelong cyclic loading, and its effects are often subject of thorough simulations or conservative estimates.

In geotechnology, two approaches to the numerical simulations of the cyclic loading are distinguished using the finite element analysis (FEA). The first, the implicit cyclic loading simulates every cycle in its full extent. The second, the explicit cyclic loading simulates only average values of cycles, and thus, in principle, constitutive models used in these analyses are related to creep constitutive models, where time t is substituted by the number of simulated cycles N. The explicit approach significantly decreases the computational time. To remedy the issue of the calculation time in the case of the implicit cyclic method, an *accelerated implicit cyclic method* can be used (Kadlicek, 2014), which is often referenced as *skipped cycles* or *cycle jump*. Benefits of this approach have not been explored for the purposes of geotechnology. In this paper, we link the acceleration of 3D mass elements with 2D interface elements in a simulation of a pile with lateral harmonic loading.

2 PRINCIPLES OF ACCELERATION

There are several approaches to the implicit acceleration. The acceleration is rooted in a simple idea of extrapolation of recorded characteristics such as strains $\boldsymbol{\varepsilon}$, stresses $\boldsymbol{\sigma}$ and other variables $\boldsymbol{q}$ forward by a desired number of cycles. In this paper, we use acceleration which is performed on two levels: global and local. On the global level, all nodal displacements $\boldsymbol{u}$ are recorded, and their linear extrapolation is used as a nodal loading during the acceleration. Processes on the global level are usually not a part of the acceleration since it requires deeper implementation beyond a simple user-defined constitutive models and subroutines. The fact that the displacements $\boldsymbol{u}$ are applied globally to all FE nodes means that the well know FEA relation

$$\mathbf{K}\boldsymbol{u} = \boldsymbol{F}, \qquad (1)$$

where $\mathbf{F}$ represents nodal forces and $\mathbf{K}$ global stiffness matrix, is fully determined. Consequently, no iterations are necessary for the acceleration, and the global stiffness matrix $\mathbf{K}$ does not have to be constructed and inverted. Recall that in every FEA, the displacements $\boldsymbol{u}$ are the variables in Eq. (1), and it is solved in every iteration and every increment of each step. As illustrated in Fig. 1, we currently use the linear extrapolation and the displacements $\Delta\boldsymbol{u}_{acl}$ which are accelerated based on the recorded displacements $\Delta\boldsymbol{u}_{rec}$ by N_{acl} number of cycles as

$$\Delta\boldsymbol{u}_{acl} = \Delta\boldsymbol{u}_{rec}N_{acl}. \qquad (2)$$

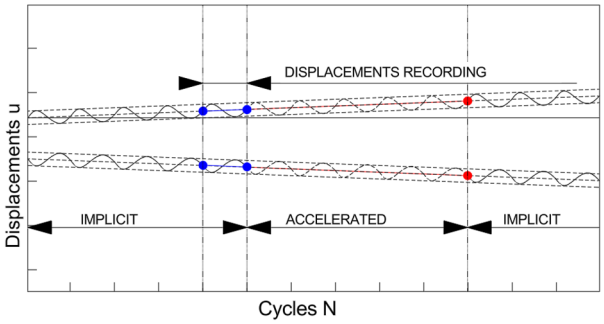

Fig. 1: Illustration of nodal displacements acceleration.

Since the global stiffness matrix $\mathbf{K}$ is not required, neither is the material stiffness matrix $\mathbf{D}$ and arbitrary stiffness can be assigned to accelerate stress tensor $\Delta\boldsymbol{\sigma}_{acl}$ on the local. Therefore, in alignment with Eq. (2) and Fig. 2, we extrapolate the recorded stress tensor increment $\Delta\boldsymbol{\sigma}_{rec}$ as

$$\Delta\boldsymbol{\sigma}_{acl} = \Delta\boldsymbol{\sigma}_{rec}N_{acl}. \qquad (3)$$

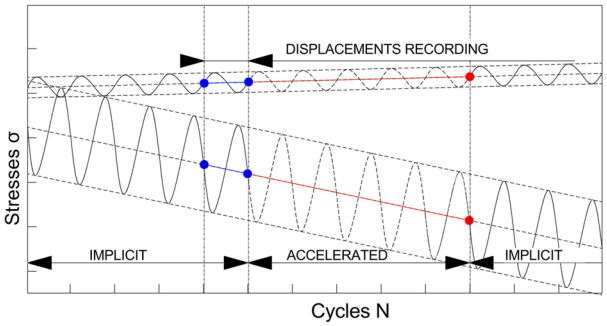

Fig. 2: Illustration of stress acceleration.

Note that the accelerated strain tensor $\boldsymbol{\varepsilon}_{acl}$ is directly evaluated from the nodal displacements based on a numerical derivation

$$\Delta\boldsymbol{\varepsilon}_{acl} = \mathbf{B}\Delta\boldsymbol{u}_{acl}, \qquad (4)$$

where **B** is a derivative of the base functions **N**.

$$\mathbf{B} = \boldsymbol{\partial}\mathbf{N}. \qquad (5)$$

The remaining state variables are accelerated equally as stresses, that is,

$$\Delta\boldsymbol{q}_{acl} = \Delta\boldsymbol{q}_{rec}N_{acl}. \qquad (6)$$

3 INTERFACE IMPLEMENTATION

The current version of the accelerated implicit cyclic method is implemented in the software Tochnog and it was initially tested on 2D and 3D mass elements only. However, to account for realistic scenarios, implementation of an interface acceleration is a crucial step. Although the aforementioned implementation works well for the user defined model of the mass elements, this approach needs to be adjusted for the interface elements. Since the goal is to allow for the soil/structure separation, we make use of the already implemented interface analysis in Tochnog, which uses penalty interface formulation. In 3D, an interface is a 2D element of zero thickness. Although an interface is a 2D element, it has double the number of nodes since it connects two opposite faces of 3D mass elements. Therefore, the global part of the implicit acceleration can be still used as all nodes of an interface will be loaded simultaneously by $\mathbf{u}_{acl}$ based on $\mathbf{u}_{rec}$.

As a constitutive model of an interface, Tochnog provides the Mohr-Coulomb model. In 3D, each interface, by default, has 3 integration points, and 3 stress components: normal stress σ_n, shear stress in the vertical direction τ_1 and shear stress in the horizontal direction τ_2. The yield surface F is defined with the friction angle φ and cohesion c as

$$F = \sigma_n \tan\varphi + c - \tau, \qquad (7)$$

where the average shear stress τ is evaluated as

$$\tau = \sqrt{\tau_1^2 + \tau_2^2}. \qquad (8)$$

Stress and strain components of each interface element are stored similarly to their mass element counterparts and extrapolated with the same extrapolation scheme

$$\Delta\sigma_{n,acl} = \Delta\sigma_{n,rec}N_{acl} \quad \text{and} \quad \Delta\tau_{acl} = \Delta\tau_{rec}N_{acl}. \qquad (9)$$

If the yield surface F is surpassed during the interface acceleration, the intersection of the stress path with the yield surface F is determined first, followed with a common *elastic predictor/plastic corrector* routine, see Fig. 3.

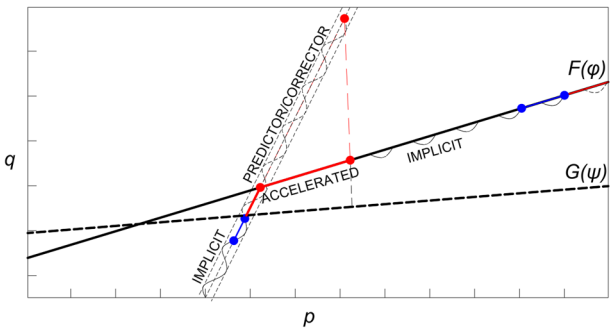

Fig. 3: Interface extrapolation with the yield surface F and the plastic potential G.

Once the acceleration of the stress components σ_n and τ is finished, individual shear stress components τ_1 and τ_2 are back calculated proportionally to their original stress ratios

$$\Delta\tau 1 = \Delta\tau acl\tau 1\tau \quad \text{and} \quad \Delta\tau 2 = \Delta\tau acl\tau 2\tau \qquad (10)$$

4 CONSTITUTIVE MODELS

In the following simulations of a laterally loaded pile, three constitutive models are used for soil, the pile and the interface. For soil, the hypoplastic sand model (Von Wolffersdorff, 1996) is used, an advanced constitutive model based on the critical state soil mechanics. This model belongs to the group of hypoplastic models which do not distinguish between elastic and plastic deformations, and evolution of its state variables are controlled by a single differential function. Model parameters used in this analysis are shown in Tab. 1.

Tab. 1: Hypoplastic sand model parameters: Soil

h_s[MPa]	n[−]	e_{i0}[−]	e_{c0}[−]	e_{d0}[−]	α[°]	β[−]	φ_c[°]
4000	0.27	0.1212	1.054	0.677	0.14	2.5	33.1

The behaviour of the pile is described by the linear elastic model. Its parameters, see Tab. 2, are selected for the concrete strength class C40/50 according to the Eurocodes 1992-1.

Tab. 2: Linear elastic model parameters: Pile

E [MPa]	ν [−]
35 000	0.2

The third constitutive model, Mohr-Coulomb model, defines the behaviour of the contact between the pile and surrounding soil. The parameters of the Mohr-Coulomb model are gathered in Tab. 3.

Tab. 3: Mohr-Coulomb model parameters: Soil/Pile interface

E [kPa]	G [kPa]	φ [°]	c [kPa]	ψ [°]
1000	750	23	0.1	5.7

5 PILE SIMULATION

The implementation of the implicit acceleration with interface elements is presented on a case of a laterally loaded pile. The simulated domain is a 100 m tall half cylinder symmetric along $x - z$ plane. Diameter of the domain is 200 m. The pile is 68 m tall and 6 m in diameter and partially embedded by 60 m. The loading is represented by a harmonic force

$$\tilde{F}_x = F_x \sin\omega N, \qquad (11)$$

where $F_x = 1{,}000$ kN, which means that 2,000 kN would be applied if the full 360° domain is considered. Geometry of the presented case is displayed in Fig. 4.

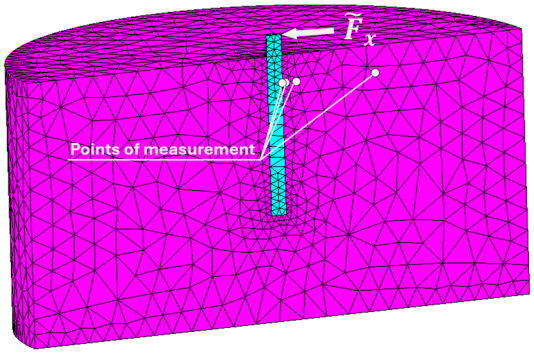

Fig. 4: Geometry of the numerical model.

Four points of measurement are defined at the depth 10 m, and distances 2.5 m, 3.5 m, 8 m and 40 m from the axis of the pile. Note that the first point is inside the pile, while the remaining points are within the body of soil. In these points, effects of the various loading intensities are observed and compared. The recorded characteristics are stresses, displacements and void ratios.

Two types of simulations of the cyclic loading were performed for 1000 cycles. First, the fully implicit cyclic loading, that is, each cycle is simulated in its full extent. This simulation thus serves as a benchmark for the accelerated simulations. In the second type of simulations, 10 implicit cycles were followed with 10 accelerated cycles in a regular sequence. These accelerated calculations were set up either with or without a simultaneous acceleration of the interface at the local level. The acceleration without accelerated interface is designated as ACL_1. This method was performed to observe what error is generated, when the interface is not accelerated on the local level. In this method the global nodal displacements are extrapolated, however, the stresses resulting from the accelerated displacements are calculated solely by the default integration of the interface constitutive model. In the second method, the acceleration of the interface stresses was performed together with the plastic corrector/predictor method. This simulation was designated as ACL_2.

5.1 *Local comparison*

In the following, the results of the simulations are compared in the four points of measurements, see Fig. 4, through displacements, stresses and void ratios.

The measurements at the distance 2.5 m are shown in Fig. 5. This point is situated inside the pile and since the pile is undergoing bending, the vertical stress σ_{zz} oscillates within a range $\Delta\sigma_{zz} \approx 4500$ kPa and gradually increases during the 1000 simulated cycles. Other horizontal stresses oscillate within lower ranges: $\Delta\sigma_{yy} \approx 550$ kPa and $\Delta\sigma_{xx} \approx 100$ kPa.

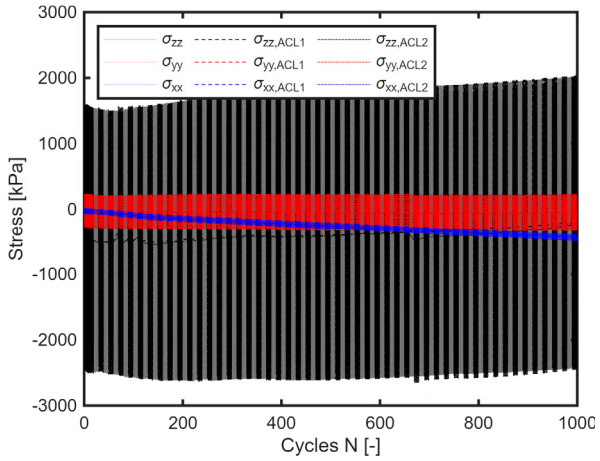

Fig. 5: Stresses evolution at 2.5 m.

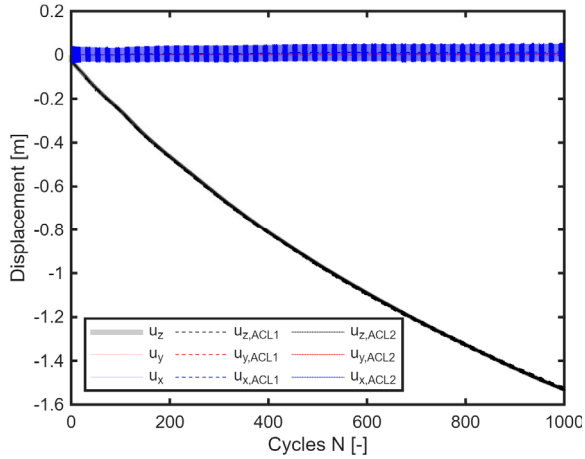

Fig. 6: Displacements at 2.5 m.

As the fully implicit simulation provides the underlaying benchmark, the accelerated simulations divergence from this trend is barely distinguishable. In the accelerated simulations, the better match with the implicit simulation is provided by ACL_2.

The maximum vertical displacement at 2.5 m obtained by the implicit calculation is $u_z = 1.5307$ m. The closest accelerated calculation is ACL_1 with $u_z = 1.5325$ followed by ACL_2 with $u_z = 1.5232$ m, see Fig. 6.

The horizontal displacement reaches $u_x = 0.0503$ m for the implicit simulation, and both the accelerated simulations deviate from this value by the maximum 0.002 m.

Stresses in Fig. 7, undergo a significant non-linear evolution during 1000 cycles. The larges divergence between the implicit and accelerated calculations can be observed at the global minimum of U-turn corresponding to 190th cycle in the case of σ_{zz} and 140th cycle in the case of σ_{yy}. The accelerated simulations follow the trend of the implicit loading in close proximity with the maximum differences reaching locally up to 30 kPa. Overall, the lowest deviation exhibits the simulation ACL_2 which often reaches less than 5 kPa from the implicit calculation. Furthermore, three significant oscillations can be observed in the 270th, 350th, and 410th cycle, which show a sudden rise in stresses during the first implicit cycle after the acceleration. These numerical artefacts are predominantly present for ACL_1, which exhibits all three such peaks, while only the first peak is present for ACL_2. It is also shown that after these peaks all accelerated calculations converge towards the implicit calculation.

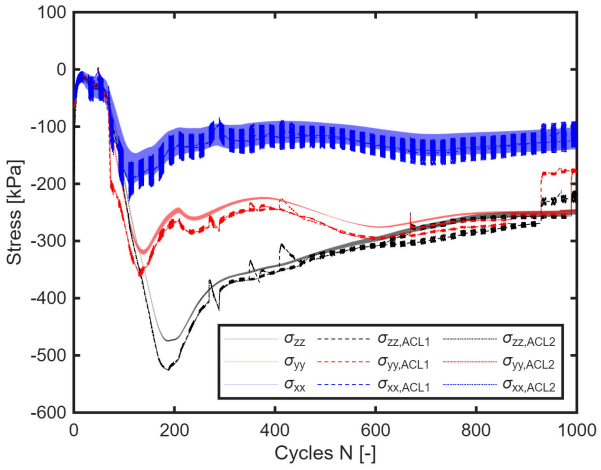

Fig. 7: Stresses evolution at 3.5 m.

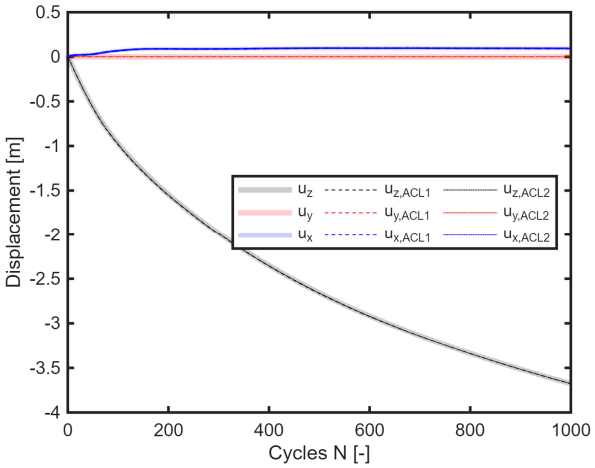

Fig. 8: Displacements at 3.5 m.

Displacements at 3.5 m are shown in Fig. 8, where $u_z = 3.6737$ m and $u_x = 0.0949$ m at 1000th cycle. The best agreement with the implicit loading in u_z is provided by ACL_2, that is, with the stress acceleration and $u_z = 3.6736$ m. ACL_1 then provides vertical displacement $u_z = 3.6750$ m. The observed differences are thus within $\Delta u_z = 0.0013$ m after 1000 cycles.

Similarly to the stresses at 3.5 m, the stresses at 8.0 m display visible nonmonotonic and highly nonlinear evolution (see Fig. 9) with the local extremes at approximately 190th and 390th cycle. The accelerated calculations follow the implicit trend very closely even around the sharp extremes. The best agreement with the implicit calculation is again provided by ACL_2, which deviates from the implicit benchmark after the 390th cycle mostly by less than 1 kPa. The calculation ACL_1 is shifted by approximately 10 kPa from the implicit calculation in the case of σ_{zz}. The jumps in stresses observed at the distance 3.5 m ale much less pronounced at this distance, while they are more significant in the case of ACL_1 than for ACL_2.

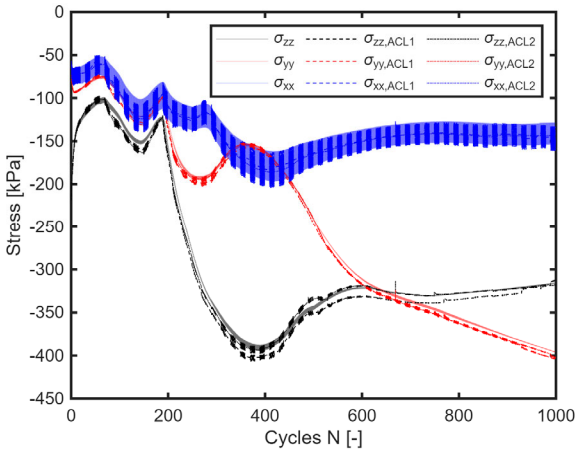

Fig. 9: Stresses evolution at 8.0 m.

The vertical displacements at 8.0 m reach in the case of implicit calculation $u_z = 3.4633$ m. ACL_1 reaches $u_z = 3.4599$ m, and in the case of ACL_1 $u_z = 3.4583$ m. All the accelerated calculations are thus within $\Delta u_z = 0.005$ m after 1000 cycles with respect to the implicit calculation.

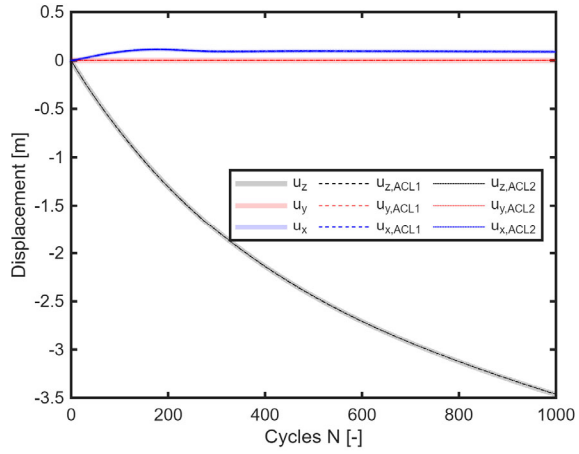

Fig. 10: Displacements at 8.0 m.

At 40.0 m, see Fig. 11, the trend of stress components is very smoothly evolving in comparison with the previous examples. Both the accelerated calculations follow the implicit calculation closely, with deviations approximately $\Delta\sigma \approx 0.2$ kPa for ACL_2 and $\Delta\sigma \approx 1.5$ kPa for ACL_1. In this case, the jumps in stresses observed at 3.5 and 8.0 vanish, and it can be reasoned that their occurrence is caused by the interface which is deformed during the acceleration together with the pile. During the subsequent implicit cycle, the pile is released which causes a sudden movement of the pile inside the interface and oscillation of stress components. This issue can be probably mitigated by more accurate prediction of stress extrapolation inside the interface. Recall, that no stress jumps are noticeable at 2.5 m. Although the jump in displacements of the soil is barely noticeable, its influence on stresses is significant due to the relatively large stiffness of soil around the pile and close proximity to the interface.

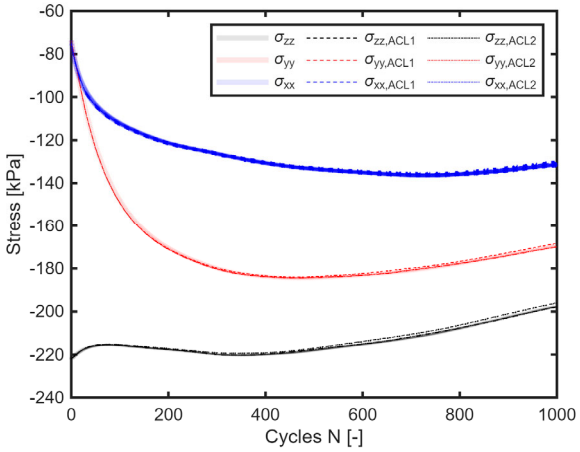

Fig. 11: Stresses evolution at 40.0 m.

Vertical displacements at 40.0 m reach a similar magnitude as at 2.5 m with $u_z = 1.5228$ m. Horizontal displacements reach larger values $u_x = 0.3182$ m. Both accelerated calculations, again, follow the implicit trend very closely, with ACL_2 being the closest calculation. Nonetheless, all calculations differ by less than 1 mm from the implicit calculation at 1000th cycle.

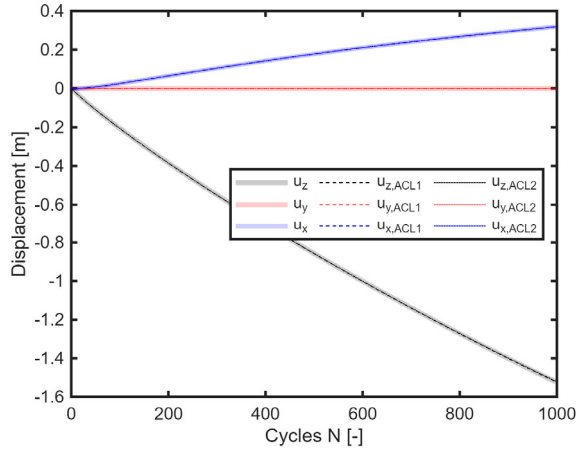

Fig. 12: Displacements at 40.0 m.

The evolution of void ratio at 3.5 m, 8.0 m, and 40.0 m is displayed in Fig. 14. Interestingly, void ratios at 3.5 m, and 8 m reach similar minimum values. Although the void ratio at 3.5 m is temporarily underestimated from 50th to 70th cycle for the accelerated calculations, they asymptotically converge towards the implicit calculation. There is not a single accelerated calculation which reaches the best agreement with the implicit calculation in all cases, however, the difference in void ratios is always relatively small with $\Delta e \approx 0.0001$, as it is closely related to the displacements.

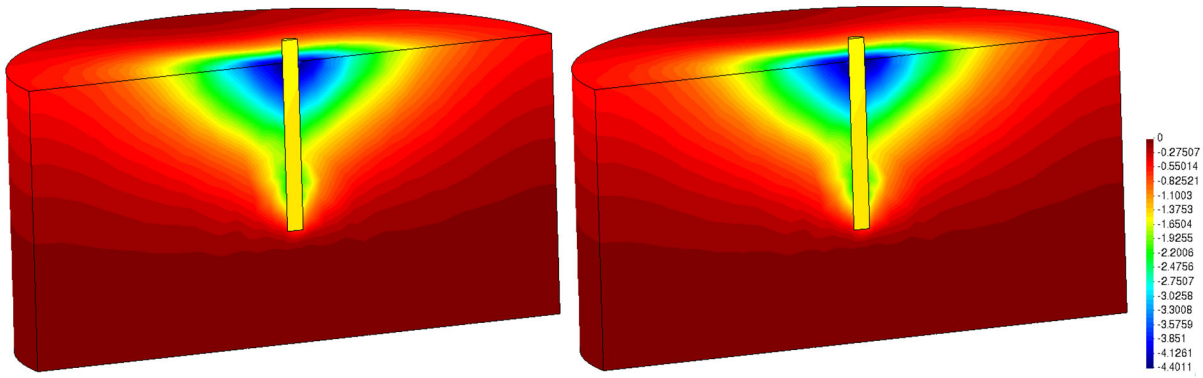

a) u_z – Implicit

b) u_z – Accelerated ACL_2

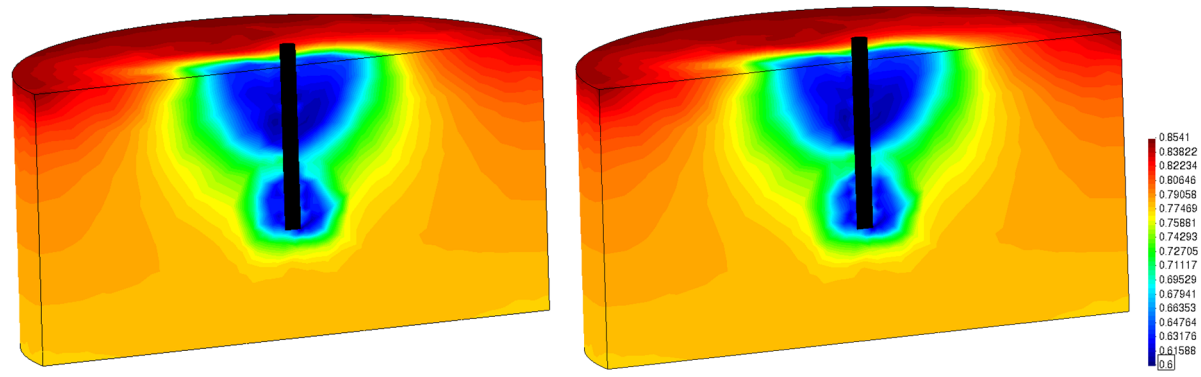

c) Void ratio e – Implicit

d) Void ratio e – Accelerated ACL_2

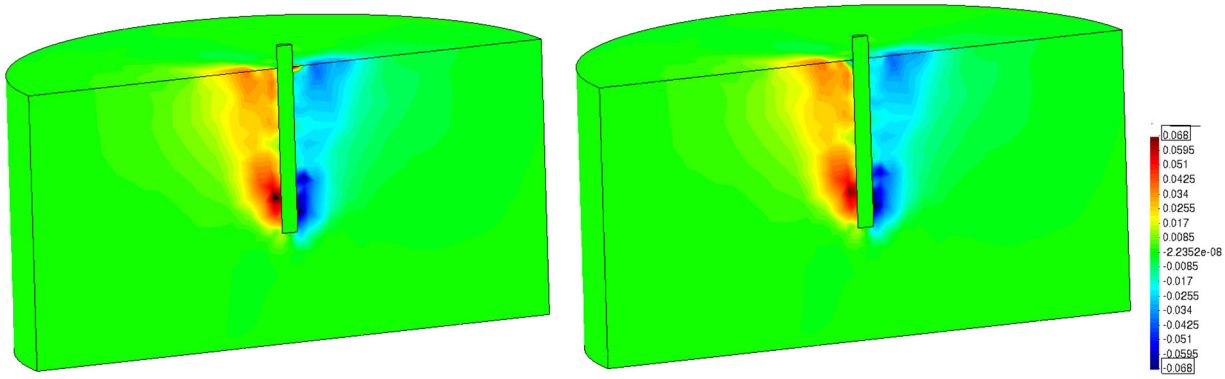

e) ε_{xz} – Implicit

f) ε_{xz} – Accelerated ACL_2

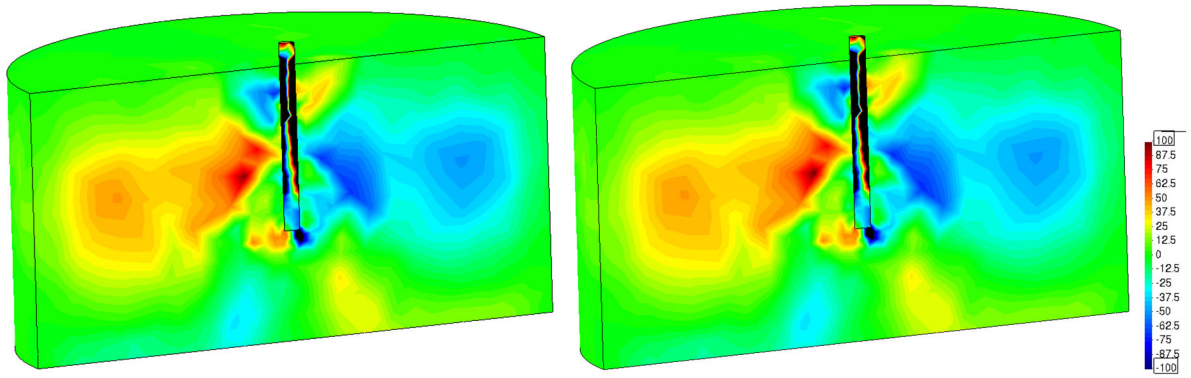

g) σ_{xz} – Implicit

h) σ_{xz} – Accelerated ACL_2

Fig. 13: Filled isolines of selected quantities for comparison.

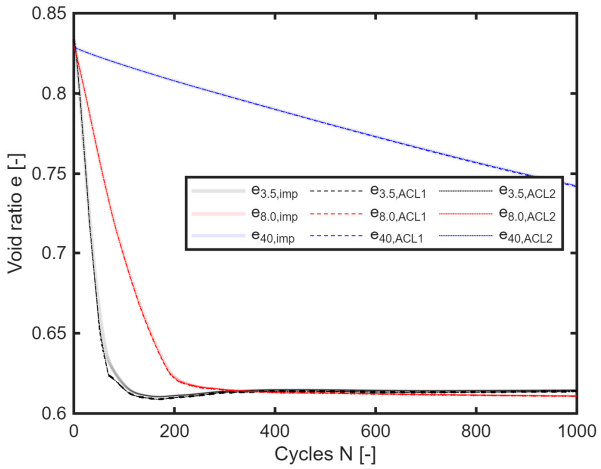

Fig. 14: Void ratios at 3.5 m, 8.0 m, and 40.0 m.

From the local observation of four points during the span of 1000 cycles, several conclusions can be drawn. First, the displacements are well established by both acceleration approaches and the differences between them are inconclusive. Second, the stress approximation of both acceleration approaches follows the implicit simulation in the close proximity. Even when the acceleration overpredicts the implicit solution, it tends to return to it. This behaviour is most probably caused by the asymptotic behaviour of the underlying constitutive model of soil, which is in this case the hypoplastic sand. Nonetheless, the best agreement with the stress benchmark was provided by the approach ACL_2 which, contrary to ACL_1, applies stress acceleration at the integration points.

5.2 *Global comparison*

Aside from the local observations, the global qualitative comparisons are shown in Fig. 13, where we compare the fully implicit calculation and the acceleration ACL_2 by means of filled isolines. To make the comparison easier, these isolines are displayed with limits on the measured characteristics for two reasons. First, the values can locally differ between the implicit and accelerated calculation in its absolute extremes which can shift colouring of the isolines. Second, the characteristics extremes in the soil and in the pile can be different by several orders of magnitude due to a significant difference is stiffness.

The first quantity in Fig. 13a and Fig. 13b is vertical settlement u_z which dominates the displacements. The width, the magnitude, and the shape of the observed settlement depression in ACL_2 agrees well with the implicit calculation. This observation is underscored by the void ratio e distribution in Fig. 13c and Fig. 13d, where the densified area around the pile head gradually transform into the background value identical to the initial void ratio. Secondary densification can be seen in both subfigures around the pile toe. The void ratio distribution matches well between both the calculations. The total shear strains ε_{xz} are displayed in Fig. 13e and Fig. 13f and indicate formation of a shear zone in the vicinity of the pile in the $x-z$ plane. Both calculations agree in the shape and the magnitude around the pile. Worth pointing out are the magnitudes of the shear deformation around the lower and upper parts of the pile. The last displayed quantity is the shear stress σ_{xz}. Again, both calculations agree well both in the shape of the distribution and the magnitude. Worth pointing out is the stress distribution in the midsection of the soil domain and around the toe of the pile.

6 CONCLUSION

In the presented study, the accelerated implicit cyclic approach was applied to cyclic loading of a pile embedded within sandy soil. The finite element analysis employed mass elements as well as interface elements between the soil and the pile. Following every 10 implicit cycles, 10 cycles were accelerated, thus decreasing the computational time by the factor of two. The results showed great agreement between the implicit and accelerated calculations.

For the acceleration, two different methods were employed: with (ACL_2) or without (ACL_1) the local stress acceleration of the interface. The results were compared locally in four points of measurement against the fully implicit simulation in terms of displacement, stress and void ratio evolutions. Interestingly, the differences between the accelerated and implicit calculations in the displacement were small, and the two acceleration methods performed equally well. This is also true in the case of void ratio e, which is dependent on the applied displacements and deformations. However, in the case of stress evolution, the simulation ACL_2, with the local stress acceleration of the interface showed better results than ACL_1, although both methods reproduced the implicit calculation satisfactorily.

In the case of stress evolution, the accelerated simulations suffered from artificial jumps during the first implicit cycle after a few acceleration instances. These are most probably caused by the movement of the pile within the interface. Although the accelerated calculations approached the implicit solution quickly after each such jump, this issue can probably be remedied by a more accurate extrapolation of stresses inside the interface as the acceleration ACL_1 was more prone to this problem than ACL_2.

Eventually, the results were also compared globally by the means of the filled isolines, which showed a remarkable agreement between the implicit and accelerated simulations, not only in the magnitude but also in the shape of the distributions.

In this analysis, three constitutive models were accelerated simultaneously and the soil/pile interface was implemented thus enabling simulations of real case scenarios in the future.

7 ACKNOWLEDGEMENT

This research was supported by the Johannes Amos Comenius Programme (OP JAC), project No. CZ.02.01.01/00/22_008/0004605, Natural and anthropogenic georisks.

8 REFERENCES

Kadlíček, T., and D. Mašín. 2014. Accelerated implicit cyclic loading with the hypoplastic sand. *Geotechnical Engineering Challenges to Meet Current and Emerging Needs of Society*. CRC Press. 3011-3014.

Niemunis, A., Wichtmann, T., & Triantafyllidis, T. 2005. A high-cycle accumulation model for sand. *Computers and geotechnics*, 32(4), 245-263.

Von Wolffersdorff, P. A. 1996. A hypoplastic relation for granular materials with a predefined limit state surface. *Mechanics of Cohesive-frictional Materials: An International Journal on Experiments, Modelling and Computation of Materials and Structures*, 1(3), 251-271.